Dynamic remodeling of the dynamin helix during membrane constriction

Adai Colom, Lorena Redondo-Morata, Nicolas Chiaruttini, Aurelien Roux, Simon Scheuring

Dynamic remodeling of the dynamin helix during membrane constriction

Classification:

Biological sciences – Biophysics and computational biology / Cell Biology

Authors:

Adai Colom[1,2], Lorena Redondo-Morata[3], Nicolas Chiaruttini[1], Aurélien Roux[1,2,§], Simon Scheuring[3,4,5,§]

[1] University of Geneva, Department of Biochemistry, 30 quai Ernest Ansermet, CH-1211 Geneva 4, Switzerland
[2] Swiss National Centre for Competence in Research Programme Chemical Biology, CH-1211 Geneva, Switzerland
[3] Unité 1006, INSERM, Aix-Marseille Université, 163 avenue de Luminy, FR-13009, Marseille, France
[4] Department of Physiology and Biophysics, Weill Cornell Medicine, New York, NY 10065, USA
[5] Department of Anesthesiology, Weill Cornell Medicine, New York, NY 10065, USA
[§] Corresponding authors: aurelien.roux@unige.ch (+41(0)22 379 35 32) and sis2019@med.cornell.edu (+1(212) 746-2954

Keywords:

dynamin, endocytosis, GTPase, high-speed atomic force microscopy, membrane fission, membrane trafficking

Abstract:

Dynamin is a dimeric GTPase that assembles into a helix around the neck of endocytic buds. Upon GTP-hydrolysis, dynamin breaks these necks (1), a reaction called membrane fission. Fission requires dynamin to first constrict the membrane (2-4). It is unclear however, how dynamin helix constriction works. Here we undertook a direct high-speed atomic force microscopy imaging analysis to visualize the constriction of single dynamin-coated membrane tubules. We show GTP-induced dynamic rearrangements of the dynamin helix-turns: the average distances between turns and between dimers along the polymer reduce with GTP-hydrolysis. However, these distances vary over time, as helical turns were observed to transiently pair and dissociate. At fission sites, these cycles of association and dissociation were correlated with relative displacement of the turns and constriction. Our findings support a model in which conformational changes at the dimer level drive relative sliding of helical turns, and constriction by torsion.

Significance Statement

The GTPase dynamin catalyzes membrane fission and is essential in endocytosis and other events such as organelle division. Dynamin is a unique molecular motor with torsional and contractile abilities. Because these abilities involve a conformational change at the whole polymer level, standard structural biology tools have not been able to fully unravel the mechanism by which it constricts and twists. Here, we used high-speed atomic force microscopy to image the constriction and fission of dynamin-coated tubules with sub-nanometer and sub-second resolution. Our results provide important findings to establish the contribution of the various constriction mechanisms.

\body

Results:

In absence of nucleotides, the molecular structure of the dynamin-1 dimer (5, 6) and dynamin-3 tetramer (7) revealed that dynamins are composed of a rigid stalk, connecting the membrane-binding Pleckstrin Homology (PH) domain to the GTPase domain (see **Fig. 1a**). In the dimer, the stalks form a cross, with the GTPase domains on one side, and the PH domains on the other. This architecture allows membrane binding through a specific interaction between the PH domains and phosphoinositide(4,5)bisphosphate (PIP_2). The GTPase domain is connected to the stalk via a flexible hinge called BSE (Bundle Signaling Element) (8, 9). The crystal structures also provided evidence how molecular interactions between dimers lead to the formation of a helical polymer (5-7). In particular, in the tetrameric form (7), GTPase domains from two contiguous dynamin dimers are closely apposed, forming a structural dimer identifiable in the helical structure (see blue-orange dimer in **Fig. 1a**). In the

following, we will call this dimer "helical dimer", as it is not equivalent to the biochemically stable dimer (**see Fig. 1a**).

Also, helical dimers from adjacent turns in the helix are closely apposed, suggesting that they may participate in molecular links between turns (see **Fig. 1a**). Cryo-EM 3D-reconstructions of dynamin helices were compatible with these models (10), even though the number of dimers per helical turn varied from 14 to 18 (7). Cryo-EM reconstructions of the dynamin helix in the presence of GMP-PCP, a non-hydrolysable GTP-analog, revealed a more constricted state with 13 to 15 dimers per turn (10-12). Altogether, X-ray and cryo-EM studies have shown that dynamin dimers undergo a conformational change leading to the constriction of the membrane tubule beneath (4, 10-13). Among these reconstructions the internal organization of dynamin domains is dramatically different: each dimer undergoes a slight rotation along the axis perpendicular to the membrane (called the "cork-screw" model in (12)), and a change of the GTPase domain positions (see **Fig. 1a**, conformational change in the "helix compaction" model). Such conformational change leads to a compaction of the polymer that could constrict the membrane (12)(see **Fig. 1a**, helix compaction). In this model, the relative position of helical dimers in adjacent turns does not change during constriction (see blue-yellow dimers in **Fig. 1a**), and molecular links between adjacent turns are conserved.

However, a super-constricted state was recently obtained with GTP and the GTPase-reduced mutant dynamin K44A (4). This structure had 11 dimers per turn, suggesting that relative sliding of adjacent turns occurred during constriction. If the helix constricts by torsion, the relative positions of helical dimers in adjacent turns change dramatically upon constriction (see **Fig. 1a**, helix torsion). Supporting this model, optical microscopy of long dynamin-coated membrane tubules showed twisting upon GTP-hydrolysis, suggesting that constriction was accompanied by torsion of the entire helix (14, 15).

In the torsion model however, transient breakage of molecular links between helix turns is required to allow for sliding and torsion. GTPase domains, which participate in molecular links between adjacent turns, would thus have to undergo cycles of dissociation/association coupled to their GTPase cycle. Crystal structures are compatible with this hypothesis: no links between GTPase domains are found in absence of nucleotide (5-7). But a truncated dynamin has been crystalized with GDP·AlF_4^- (8), a nucleotide mimicking the hydrolytic state of GTP in dynamin, and in this state, GTPase domains interact strongly (termed 'G-G link' in the following). Also the BSE moves by an angle of approximately 70° relative to the nucleotide-free structure, suggesting that the GTPase domains generate a powerstroke driving turn sliding and torsion upon GTP-hydrolysis (13).

While torsion and compaction are not exclusive, as both mechanisms could occur at the same time in constriction, we ought to test the torsion model by visualizing the global conformational changes of single dynamin-coated membrane tubules with molecular and sub-second resolutions: we adapted *in vitro* reconstitution assays for high-speed atomic force microscopy (HS-AFM (16)) that has recently proven powerful for the study of membrane remodeling proteins on mica-supported bilayers (17). We

found that the adhesion of the proteins to the mica could impair the dynamin helix conformational change. To overcome this technical limitation, we coated the mica with biotin-lipid bilayers and attached partially (10%) biotinylated dynamin tubules via streptavidin. We reasoned that one tenth of the dynamins being biotinylated, we would have in average about one functionalized dynamin per helix turn, and hence anchorage of the tubules to the support about every ten turns. This strategy generates links strong enough to avoid displacement of the tubules during HS-AFM scanning, but spreads attachment points far enough for providing motional freedom (18) and allowing to observe conformational changes of the dynamin-helix (**see Methods for details**).

First experiments were performed with 100% di-oleyl-phosphatidylserine (DOPS) liposomes (2) mixed with ΔPRD (deleted-Proline-Rich-domain) human dynamin-1 expressed and purified from bacteria (5). 100% DOPS was used as it favored the formation of long dynamin-coated tubules in electron microscopy assays (2, 3). We confirmed that ΔPRD-dynamin bound to DOPS liposomes and deformed them into long membrane tubules decorated by a dynamin helix (**Fig. 1b-c**), as previously observed (2, 19). ΔPRD-dynamin was used instead of full-length dynamin because absence of the flexible PRD-domain resulted in better resolution in HS-AFM images (see **Fig. S1a,b**). The average thickness of these tubules was 63.0 ± 10.4 nm (N = 28) (mean ± SD, as throughout the article, unless noted) and the pitch of the striations was 19.2 ± 3.6 nm (N = 141 turns on 4 tubules, see **Fig. 1c**). We measured similar values in EM images (diameter: 59.0 ± 4.5 nm; N = 26, pitch: 15.0 ± 4.5 nm, N = 38 tubules), consistent with previous reports (2). It is noteworthy that HS-AFM contours only the protein surface, which in the case of dynamin is composed of helical dimers. Whenever we refer in the following to dimers, we examine the structure and position of these surface exposed domains – helical dimers – and cannot provide information about intramolecular conformational changes.

We then added 10µl of a 10mM GTP-solution to the 90µl fluid chamber volume, resulting in 1.1mM GTP. Right after GTP-addition, we often observed tubules constriction (see **Fig. 1b-d, Movie S1**, **Fig. S1c-h**). Constriction, however, appeared very inhomogeneous, with some parts remaining unconstricted and others narrowed. This constriction was not due to forces applied by the AFM tip onto the tubule, as the same constriction was visible on other tubules when the field of observation was widened (compare **Fig. 1b** with **Fig. 1d, Fig. S1c** with **S1e, Fig. S1g** with **S1h**). As well, the constriction was also observed in the more physiological conditions in which full-length dynamin was used to generate tubules out of liposomes formed of brain extract lipids supplemented with 15% PIP_2 (**Fig. S1i**). The dynamin-coat remained mostly attached, and striations were visible during the constriction of the tubules, even though the regularity of the pattern was strongly affected (**Fig. 1c, Fig. S1d, f**). At some of the most constricted locations, the tubule was virtually invisible, suggesting that fission may have occurred at these sites (**Fig. 1c and Fig. S1,** orange arrowheads).

In order to achieve higher temporal resolution imaging of the constriction, we acquired HS-AFM movies at 0.96s/frame (**Fig. 2a, Movie S2**) and 1.5s/frame (**Fig. 2b, Movie S3**). When GTP was added to the observation chamber, a slow constriction of the

dynamin-coated tubules was observed (see **Fig. 2a-c, Fig. 2f-g, Fig. S2a-c**). Such continuous constriction of tubules was never observed in the absence of GTP (**Fig. 2h)** or after addition of GDP·AlF_4^- (**Fig. S3a-c)**. A minor, homogenous constriction was observed in the presence GMP-PCP (**Fig. S3d-h**), consistent with the cryo-EM data that showed a more constricted state when ΔPRD-dynamin was loaded with GMP-PCP (10, 11).

Upon GTP-addition, the initial tubule thickness of 60-70 nm reduced to 20-30 nm in the most constricted sites (**Fig. 2f-g, Fig. S2a-c**). As compared to previous estimates of the constriction dynamics of 0.5-1 s (15), the slow constriction dynamics observed in these movies is most probably due to friction with the surface and steric hindrance caused by the streptavidin/biotin bonds, as some tubules showed faster constriction upon a single GTP-addition (e.g. **Fig. 1c**). However, these movies have lower resolution, which suggests that these tubules have fewer bonds with the surface, being freer to move. But the continuous, slow constriction observed (**Fig. 2a-b, Movies S2-3**) argues for an active process triggered by multiple cycles of GTP-hydrolysis, rather than an abrupt, single-event conformational change.

After the slow progressive constriction of the entire tubule, a more rapid reduction of the tubule thickness at the most constricted locations was observed (see between time 40 and 50 min in **Fig. 2f**). However, the HS-AFM tip still recorded a height of about 18-23 nm in these locations (**Fig. 2g**). This could be explained by highly curved but not broken membrane tubules, or remains of the dynamin coat attached to streptavidin onto the supported bilayer after fission. The height of the dynamin/streptavidin/lipid complex generated for anchoring the tubules to the mica surface is in the range of 15-20 nm (**Fig. S4**). We thus concluded that fission had occurred and that the remaining measured height corresponded to remnants of the dynamin coat at the fission site still linked to the supported bilayer on the mica.

Interestingly, in some constricted parts of the tubule, the resolution was high enough to resolve the helical turns of dynamin (**Fig. 2d, Fig. S2d; Fig. S2e**). Our observations show that fission occurred where the helical turns are the most constricted (**Fig. 2d, Fig. S2d**). Due to limitations of how far the tip can penetrate between dynamin turns, it is not detectable in these images whether partial disassembly occurred at the fission site or not. It is however clear that highly constricted turns are in close vicinity to the fission site, and that the depth within the fission site is significantly deeper than the one of the surrounding constricted turns (**Fig. 2d,** end of kymograph). Thus, fission clearly occurred where the curvature gradient along the tubule axis was highest, as previously proposed (20).

During constriction of the tubule, the helical pattern remained visible most of the time (**Fig. 2d, Fig. S2d**). Interestingly, some of the helical turns moved apart, some seemed to collapse into a single turn and/or split upon GTP addition, which we interpret as pairing and dissociation of neighboring turns (arrows in **Fig. 2a and d**, see also **Fig. 4a**). Moreover, the 'intensity', i.e. the height of the turns, greatly varied with time, as expected during constriction. On the contrary, neither lateral rearrangements nor height variations were observed in the absence of GTP (**Fig. 2e**), nor in the presence of GMP-

PCP or GDP·AlF_4^-. Importantly, these variations and rearrangements are unrelated to fluxes occurring in the chamber upon GTP addition, as they did not occur upon buffer addition. We quantified these rearrangements: On average, the helix pitch reduced from 19.2 ± 3.6 nm (N = 141) to 15.2 ± 4.9 nm (N = 38) (**Fig. 2i**), consistent with the helix height profile showing closer turns (**Fig. 2j**), yet the standard deviation, *i.e.* the variability of the pitch, increased. Along with this helix shortening, we observed a significant change of turn lateral thickness (see blue arrows in **Fig. 2d**). This could be due to turn pairing, as described above, or to a change of the angles between turns and the tubule axis: from a sharp distribution around 90°-95° in absence of GTP, the angles spread from 50° to 105° with GTP (**Fig. 2k**). This change of orientation was highly dynamic (**Fig. 2a,** orange arrow**, Fig. S2e**). Altogether, our results show that GTP-hydrolysis changes a rather regular helix into a highly dynamic and variable structure on the way to fission, a behavior that could not be pictured by the previous static, averaged structures of crystallographic and cryo-EM data.

The resolution of the images on DOPS tubules was however insufficient to visualize the details of the helical reorganization process at the single protein level, most probably because DOPS tubules have a low rigidity limiting HS-AFM resolution (16, 21). To improve HS-AFM contouring and thus the resolution of the images, we opted for the use of rigid lipid nanorods formed by the spontaneous assembly of galactocerebrosides (22, 23). Galactocerebrosides were supplemented with 5% PIP_2 to mediate dynamin binding to the nanorods (22). Nanorods are rigid and cannot be constricted by dynamin. Indeed, once assembled onto these templates in absence of GTP (**Movie S4**), substructures of the helix were resolved (**Fig. 3a**): the pitch of the helix was 15.4 ± 2.9 nm (**Fig. 3b**) similar to previous estimates (2, 3, 10, 22), a bit shorter than on the DOPS tubules (**Fig. 2i**). Along the helical path, we observed rigid bodies (**Figs. 3a** and **4a**) that we interpreted as helical dimers, spaced by 12.7 ± 2.3 nm. Moreover, molecular links bridging adjacent turns at the position of each rigid body, of the helix were clearly resolved (**Fig. 3a,** arrow). We interpreted these links as G-G links, between adjacent helical dimers (8).

We then added GTP to these dynamin-coated nanorods during HS-AFM imaging. We never observed constriction, however, strong modifications of the dynamin helix occurred. On average, the pitch of the helix shortened by about 30% upon GTP-addition (**Fig. 3b**). But the well-preserved periodicity of the helix in absence of GTP, was lost upon GTP-addition: in some cases, we observed a shortening of the peak-to-peak distance in the helix height profile (**Fig. 3c, Movie S5**) similar to what was seen on DOPS tubules (**Fig. 2i**). In other cases, height profiles showed increasing distances between peaks after GTP-addition (**Fig. 3d, Movie S6**), consistently with a previous report that the helix pitch was larger after GTP-hydrolysis on nanorods (22). To explain this variability within our observations, we checked by negative stain EM how dynamin-coated nanorods behaved upon GTP-treatment. As previously reported (22), we observed helices with increased pitch distance (**Fig. S5a,b**), but we also found compacted helices with a shorter pitch (**Fig. S5c**), consistent with the pitch reduction observed by HS-AFM (**Fig. 3b, c**).

Altogether, these observations show strong dynamics of dynamin helical turns during GTP-hydrolysis. Indeed, we were able to observe adjacent turns undergoing dynamic cycles of association/dissociation in presence of GTP (**Fig. 4a**), but we cannot provide statistics whether more than two neighboring turns can be clustered by such pairing**.** These observations are consistent with the pairwise collapse and separation of helical turns observed on DOPS tubules (**Fig. 2d**). This dynamical breathing of the dynamin helix turns suggests that the G-G-links can be either tighter, causing the apparent pairing of two adjacent turns, or looser, causing turns to separate, in the presence of GTP (**Fig. 4a,** white arrows)**.** However, we cannot exclude that these cycles of association/dissociation are not random collisions, as we could not observe molecular links between helical dimers in all experiments.

Our results on the dynamic changes observed in the pitch and angle of helical turns show that the constriction observed on membrane tubules is correlated with processive cycles of helical turns pairing and separating, probably consecutive to conformational changes at the level of each dimer. Importantly, the dynamical breathing of dynamin turns described above is an essential postulate of the torsion model (see **Fig. 1a**): this model implies that dynamins in neighboring turns must dissociate to allow constriction, slide and reassociate to perform constriction.

However, we also noticed that the distances between helical dimers along the helical path reduced upon GTP-addition (**Fig. S5d**). The distribution of these distances changed from a single peak distribution centered on 12-14 nm in absence of GTP to a heterogeneous distance distribution with two apparent peaks in presence of GTP, one around 6-10 nm and the other remaining at 12-14 nm (**Fig. S5d**). This change of distances could be the result of GTPase domains powerstroke upon GTP hydrolysis, as in the torsion model GTPases domains have been proposed to slide turns relatively through a myosin-like mechanism (24). But this change of distances could also be the result of a helix compaction following a cork-screw intramolecular conformational change (see **Fig. 1a** and (12)). We thus looked for further evidence of relative displacement of adjacent helical turns.

As nanorods do not allow constriction, we looked for evidences of turn relative displacement on DOPS tubules. Although DOPS tubules are softer than nanorods, occasionally helical dimers were visible (**Fig. 2b**, fission point 1 (F.P.1), at higher magnification in **Fig. 4b**) in particular when the tube was already highly constricted and therefore probably more rigid. Close to fission sites, the evenly spaced helical dimers moved with respect to each other in adjacent turns (**Fig. 4b**): While the topographic heights – interpreted as helical dimers – are basically aligned facing each other at t=0min03s (**Fig. 4b**, red and blue outlines), the same are later (t=156s) in a clearly non-aligned zig-zag arrangement. Also, the profiles show that these lateral movements are associated with a reduction of the height of the turns, and thus with constriction (**Fig. 4b,** profiles). These results evidence the relative displacement of helical dimers from neighboring turns, but does not clearly show relative sliding of turns over a distance larger than the size of a helical dimer.

To provide further evidence for this lateral sliding, we undertook another approach: We ought to visualize dynamin oligomer displacements on the surface of a supported lipid bilayer. We noticed however that ΔPRD-dynamin hardly formed oligomers at the surface of mica-supported bilayers (**Fig. S6a**), most probably, because the substrate is too rigid to allow for a minimal bending of the membrane required for dynamin oligomerization. To overcome this problem, we thought of using two stacked membranes instead of one, expecting the top membrane to be more deformable. The first layer was generated by vesicle-fusion of positively charged GUVs (containing DOTAP) onto the mica, onto which we added negatively charged GUVs (containing DOPS). As expected, ΔPRD-dynamin bound specifically to negatively charged lipids (**Fig. S6b**). Indeed, negative stain EM of these dynamin-coated surfaces showed a striking assembly of short disordered dynamin oligomers (**Fig. 4d**). GTP-treatment produced an increase of the fluorescence signal in absence of soluble dynamin (**Fig. S6b**, panel +GTP). This increased fluorescence signal could be related to clustering of short oligomers. In agreement, EM showed aggregation of oligomers after GTP-addition (**Fig. 4c**, panel +GTP). Further support for this came from AFM nanomechanical measurements (**Fig. S6c and e**), that showed an increased rigidity from 59 MPa ±18 MPa to 130 MPa ± 43 MPa of the dynamin-coated membrane after GTP-addition, consistent with the formation of clustered dynamin structures on the membrane.

We then studied the dynamics of dynamin oligomers on these double-stacked supported bilayers upon GTP-addition using HS-AFM (**Fig. S6d,e**). Even though we could not resolved single dynamin oligomers, we observed displacements of elongated structures from large protein domains (**Fig. 4d, Fig. S7a,b, Movies S7,8**). We interpreted these movements as resulting from the sliding of the short dynamin oligomers relative to each other. The movements of the dynamin chains could change direction over time (**Fig. 4d**, kymograph). These observations are in further support that GTP may lead to relative lateral displacement between adjacent dynamin oligomers.

Our study shows that GTP-hydrolysis induces striking changes in the helical structure of assembled dynamin: First, adjacent helix turns can transiently dissociate and reassociate, probably through transient unbinding of G-G links. Second, the helix constricts concomitantly with these molecular rearrangements. However, this constriction is not homogeneous, which may be linked to the difficulty of propagating the constriction along the length of long helices (15). Third, fission occurs where constriction is the strongest, consistent with previous findings (20). Also, we did not observe any detectable disassembly of the dynamin coat upon GTP-hydrolysis, which may question that disassembly is an important step of the fission reaction (24). Our results are thus in support of a model where the GTPase domains transiently interact to induce a powerstroke upon GTP-hydrolysis, driving turn sliding and constriction through torsion (25, 26). However, our study of the dynamics of the topographic surface of dynamin tubules does not provide any information about internal rearrangements of the dynamin coat, leaving entirely open the possibility that this torsion is accompanied by a compaction of the polymer.

Materials and methods:

Lipid suspensions

All lipids were purchased from Avanti Polar Lipids, the galactocerebrosides from Sigma.

Large Unilamellar Vesicles (LUVs). Vesicles were prepared using 100% 1,2-dioleoyl-*sn*-glycero-3-phospho-L-serine (DOPS) or DOPS:1,2-dioleoyl-*sn*-glycero-3-phosphoethanolamine-N-(cap biotinyl) (Biotinyl Cap PE) 90:10, mol:mol, mixture or 1,2-dipalmitoyl-*sn*-glycero-3-phosphocholine (DPPC):Biotinyl Cap PE 90:10, mol:mol, mixture. Lipids dissolved in chloroform were dried under N_2 flux, followed by 30' incubation in a vacuum oven at 30°C or 2h in a desiccator. Hereafter, lipids were fully rehydrated with GTPase buffer (20 mM HEPES, 150 mM NaCl, 5 mM $MgCl_2$ at pH 7.4) for 10 min at RT, obtaining a 2.5 mg/ml lipid solution. Finally, the lipid suspension was vortexed for 10 s and freeze-thawed three times in liquid nitrogen and a water bath, respectively.

Nanorods. The lipid composition of the nanorods is: galactocerebrosides:L-α-phosphatidylcholine (Egg PC):L-α-phosphatidylinositol-4,5-bisphosphate (PI(4,5)P2):cholesterol:Biotinyl Cap PE 40:40:10:9:1 mole ratios. The nanorod lipid mix was dried under N_2 flux, followed by 30 min under vacuum at 30°C (Thermo Scientific Heraeus) or 2h in a desiccator to allow completely solvent evaporation. After, GTPase buffer was added to rehydrate the lipids for 10 min at RT to a final concentration of 2.5mg/ml. The mixture was vortexed for 10 s and sonicated for 10 min in a bath sonicator. In the end, a tip sonicator (Active Motif) was applied to the solution during 2 s at 60W and 20kHz.

Giant Unilamellar Vesicles (GUVs). Giant Unilamellar Vesicles (GUVs) were composed of 100% DOPS or 100% 1,2-dioleoyl-3-trimethylammonium-propane (DOTAP). GUVs were prepared by electroformation. Briefly, 20 µL of 1 mg/mL lipid solution were deposited on two indium tin oxide (ITO)-coated glass slides (70-100 Ω surface resistivity, from Sigma) and vacuum dried. A ~1 mm thick O-ring was used as spacer to form a chamber between the two ITO slides, which was filled with 200 mM sucrose and exposed to 1V AC-current with a 10 Hz sinusoidal wave for 1 h. The resulting GUVs suspension was carefully harvested and used within the same day.

Dynamin-coated lipids preparation. For the lipid tubulation with dynamin, 5 µl of LUVs suspension were mixed with 2 µl (0.9 mg/ml) of ΔPRD-dynamin (containing 10% of biotinylated-ΔPRD-dynamin) and 10 µl of GTPase buffer during 30 min at RT. For the dynamin-coated nanorods, 5µl of nanorods suspension were used for the reaction instead.

Supported lipid bilayers. For mica-Supported Lipid Bilayers (SLBs), LUVs composed of DPPC:Biotinyl Cap PE 90:10, mol:mol, were deposited onto freshly cleaved mica, incubated for 15 min and rinsed thoroughly with GTPase buffer. For the formation of

two-stacked SLBs, the sample was prepared by first depositing DOTAP GUVs on a freshly cleaved mica disk. After the Supported Lipid Bilayer was formed, the sample was carefully rinsed with GTPase buffer. Then, DOPS GUVs were deposited, forming a double bilayer, the closest to the mica being the DOTAP bilayer and the farthest the DOPS bilayer. After rinsing with GTPase buffer, ΔPRD-dynamin was added to give a final concentration of 0.22 mg/ml, incubated for 30 min and then rinsed again with GTPase buffer before imaging.

High-Speed atomic force microscopy (HS-AFM) images. A HS-AFM SS-NEX (RIBM, Japan) (27) setup was equipped with short (7μm long and 2μm large) cantilevers with nominal spring constant of 150 pN nm^{-1}, resonance frequency of about 600 kHz and a quality factor $Q = 1.5$ in liquid (Nanoworld), was used for movie acquisition. The microscope was operated in amplitude modulation mode, where the cantilever oscillates at a frequency close to its resonance frequency. The phase-shift in the oscillation of the cantilever is used to create the phase images, which provide information about the viscoelastic properties of the material. Herein, both topographic and phase images are reported. Either bare mica or mica covered by DPPC:Biotinyl CAP PE, 9:1, mol:mol, SLBs were used as support, in the latest followed by the addition of 0.1 μM streptavidin. Streptavidin was incubated for 5 min and rinsed 10 times with GTPase buffer. Finally, the dynamin-DOPS tubule sample was added and incubated for 30 min at RT. During imaging, GTP, GDP·AlF_4^- or GMP-PCP solutions were added directly to the HS-AFM fluid cell, if indicated. HS-AFM movies were analyzed in ImageJ, self-written analysis routines and WSxM 5.0 software (Nanotec (28)).

Quantitative nanomechanical mapping. The AFM fluid cell contained 100μL of GTP buffer. After imaging in the absence of GTP, GTP solution was added through the inlet of the AFM fluid cell to give a final concentration of ~ 2.5 mM.

Nanomechanical measurements were performed on a Nanoscope-V AFM (Bruker, Santa Barbara, CA, USA) equipped with Nanoscope-8 control software, in Peak-Force Quantitative-Nanomechanics (PF-AFM) mode. We used Si_3N_4 cantilevers with a nominal spring constant of 150 pN nm^{-1} and silicon tips with a nominal radius of 2 nm (MSNL, Bruker, Santa Barbara, CA, USA). The actual spring constant of the cantilever was determined using the thermal fluctuation method (29). Images were obtained at a resolution of 512 by 512 pixels at a line scan rate of 1 Hz. In PF-AFM, the sample support is oscillated at a constant rate (2 kHz) and amplitude (15 nm). Monitoring the cantilever deflection in each oscillation cycle allows to obtain a force-distance curve on each pixel of the image. The approach trace was used to control the maximum force applied (~300 pN). The retract trace was used to determine the Young's modulus by fitting the Hertz model of a spherical tip of radius R indenting an elastic half-space:

$$F = \frac{4E}{3(1-\nu^2)}\sqrt{R}\delta^{3/2}, \qquad \text{(equation 1)}$$

where F is the force applied, ν is the Poisson ratio (assumed 0.5 as for a perfectly elastic uncompressed material) and δ the indentation. The tip radius was assumed 2 nm, its nominal radius. To avoid contributions from long-range electrostatic forces and short-

range van der Waals interactions, the Hertz model fit was restricted to a range between 30% and 90% of the maximum F. Image and data processing was performed using Gwyddion 2.38 open software (gwyddion.net).

Acknowledgements:

The authors would like to thanks Oliver Daumke, Pierre-Emmanuel Milhiet, Peter Hinterdorfer for their appreciable comments on the manuscript. The Scheuring group acknowledges funding support from: ANR grants, ANR-Nano ANR-12-BS10-009-01 and ANR-BBMS ANR-12-BSV8-0006-01, and a European Research Council (ERC) starting (consolidator) grant #310080-MEM-STRUCT-AFM. The Roux group acknowledges funding support from: Human Frontier Science Program (HFSP), Young Investigator Grant #RGY0076-2008: the European Research Council (ERC), starting (consolidator) grant #311536-MEMFIS: the Swiss National Fund for Research, grants #131003A_130520 and #131003A_149975.

References:

1. Ferguson SM & De Camilli P (2012) Dynamin, a membrane-remodelling GTPase. *Nat Rev Mol Cell Biol* 13(2):75-88.
2. Sweitzer SM & Hinshaw JE (1998) Dynamin undergoes a GTP-dependent conformational change causing vesiculation. *Cell* 93(6):1021-1029.
3. Danino D, Moon KH, & Hinshaw JE (2004) Rapid constriction of lipid bilayers by the mechanochemical enzyme dynamin. *J Struct Biol* 147(3):259-267.
4. Sundborger AC, *et al.* (2014) A dynamin mutant defines a superconstricted prefission state. *Cell reports* 8(3):734-742.
5. Faelber K, *et al.* (2011) Crystal structure of nucleotide-free dynamin. *Nature* 477(7366):556-560.
6. Ford MG, Jenni S, & Nunnari J (2011) The crystal structure of dynamin. *Nature* 477(7366):561-566.
7. Reubold TF, *et al.* (2015) Crystal structure of the dynamin tetramer. *Nature* 525(7569):404-8.
8. Chappie JS, Acharya S, Leonard M, Schmid SL, & Dyda F (2010) G domain dimerization controls dynamin's assembly-stimulated GTPase activity. *Nature* 465(7297):435-440.
9. Gao S, *et al.* (2010) Structural basis of oligomerization in the stalk region of dynamin-like MxA. *Nature* 465(7297):502-506.
10. Chen Y, Zhang P, Egelman E, & Hinshaw JE (2004) The stalk region of dynamin drives the constriction of dynamin tubes. *Nat Struct Mol Biol* v11(n6):574-575.
11. Zhang P & Hinshaw JE (2001) Three-dimensional reconstruction of dynamin in the constricted state. *Nat Cell Biol* 3(10):922-926.
12. Mears JA, Ray P, & Hinshaw JE (2007) A corkscrew model for dynamin constriction. *Structure* 15(10):1190-1202.
13. Chappie JS, *et al.* (2011) A pseudoatomic model of the dynamin polymer identifies a hydrolysis-dependent powerstroke. *Cell* 147(1):209-222.
14. Roux A, Uyhazi K, Frost A, & De Camilli P (2006) GTP-dependent twisting of dynamin implicates constriction and tension in membrane fission. *Nature* 441(7092):528-531.

15. Morlot S, Lenz M, Prost J, Joanny JF, & Roux A (2010) Deformation of dynamin helices damped by membrane friction. *Biophys J* 99(11):3580-3588.
16. Ando T, Uchihashi T, & Scheuring S (2014) Filming Biomolecular Processes by High-Speed Atomic Force Microscopy. *Chemical Reviews* 114(6):3120-3188.
17. Chiaruttini N, *et al.* (2015) Relaxation of Loaded ESCRT-III Spiral Springs Drives Membrane Deformation. *Cell* 163(4):866-879.
18. Kodera N, Yamamoto D, Ishikawa R, & Ando T (2010) Video imaging of walking myosin V by high-speed atomic force microscopy. *Nature* 468(7320):72-76.
19. Takei K, Slepnev VI, Haucke V, & De Camilli P (1999) Functional partnership between amphiphysin and dynamin in clathrin-mediated endocytosis. *Nat Cell Biol* 1(1):33-39.
20. Morlot S, *et al.* (2012) Membrane shape at the edge of the dynamin helix sets location and duration of the fission reaction. *Cell* 151(3):619-629.
21. Colom A, Casuso I, Rico F, & Scheuring S (2013) A hybrid high-speed atomic force–optical microscope for visualizing single membrane proteins on eukaryotic cells. *Nat Commun* 4:2155.
22. Stowell MH, Marks B, Wigge P, & McMahon HT (1999) Nucleotide-dependent conformational changes in dynamin: evidence for a mechanochemical molecular spring. *Nat Cell Biol* 1(1):27-32.
23. Marks B, *et al.* (2001) GTPase activity of dynamin and resulting conformation change are essential for endocytosis. *Nature* 410(6825):231-235.
24. Antonny B, *et al.* (2016) Membrane fission by dynamin: what we know and what we need to know. *EMBO J* 35(21):2270-2284.
25. Morlot S & Roux A (2013) Mechanics of dynamin-mediated membrane fission. *Annual review of biophysics* 42:629-649.
26. Roux A (2014) Reaching a consensus on the mechanism of dynamin? *F1000prime reports* 6:86.
27. Ando T, *et al.* (2001) A high-speed atomic force microscope for studying biological macromolecules. *Proc Natl Acad Sci U.S.A* 98(22) :12468-72.
28. Horcas I, *et al.* (2007) WSXM: A software for scanning probe microscopy and a tool for nanotechnology. *Review of Scientific Instruments* 78(1).
29. Hutter JL & Bechhoefer J (1993) Calibration of atomic-force microscope tips. *Review of Scientific Instruments* 64(7):1868-1873.

Figures legends:

Fig. 1) HS-AFM imaging of dynamin-coated tubules. a) Two proposed models of dynamin constriction. Top left: basic structural features of the dynamin dimer and of the tetramer: blue and orange GTPase domains from 2 adjacent dynamin dimers form the "helical dimer", a visible unit in the helical form. Bottom left: helix assembly of the dimers. Bottom right: compaction model (schematic but not precise representation of dimer conformational changes, see (12) for details). Top right: Torsion model: The relative movement of helix turns is highlighted by the relative displacement of the blue-yellow dimers interacting in the non-constricted state. **b)** DOPS tubule with polymerized ΔPRD-dynamin before GTP-addition. **c)** Image sequence during GTP-hydrolysis of the area outline by dashed rectangle in b) and d). 0s is the time of GTP-injection. White arrowheads point at a constriction site. Orange arrowheads point at a fission site. **d)** ΔPRD-dynamin-DOPS tubule shown in b), after GTP-addition.

Fig. 2) Constriction and fission of dynamin-coated tubules observed by HS-AFM. a) Image sequence of ΔPRD-dynamin-coated tubules, adsorbed on a mica-supported bilayer (see Supplementary Methods). During the experiment, GTP was injected twice, and the dynamin helix conformational change monitored as a function of time. White arrowheads point at constriction sites, orange arrowhead at fission sites. **b)** Another example similar to a), with three consecutive GTP-injections. White arrowheads point at a constriction site, which later became fission sites (indicated by F.P.1 (fission point 1) and F.P.2 (fission point 2)). **c)** Kymograph along the dashed line F.P.1 in b). Red dashed lines indicate GTP-additions. **d)** Helix profile kymograph along the long tubule axis (dashed line labeled 'd' in image b), crossing F.P.2) revealing morphological changes of the dynamin helix. Arrows point at turn height reduction consistent with constriction (white), lateral separation of adjacent turns (green), collapse of two turns in one (red), turn enlargement (blue), and fission (yellow). **e)** Kymograph along the axis of a tubule not treated with GTP. **f**) Maximum height of F.P.1 and F.P.2 as a function of time in b). **g)** Height profile along the dashed line at F.P.1 in b) before GTP-addition and after the third GTP-addition. **h)** Maximum height of a tubule not treated with GTP as a function of time. **i)** Distribution of dynamin helix pitch distances before GTP-addition (grey bars, 19.2±3.6nm; mean±SD, *N*=4) and after GTP-addition (red bars, 15.2 ± 4.9 nm; mean ± SD, *N*=2). **j)** Height profiles of the dynamin helix along the tubule axis shown in Fig. 2B before (grey) and after (red) GTP-addition. **k)** Dynamin helix turn angle (with respect to the long tubule axis) before (grey) and after (red) GTP-addition (from movies shown in panels a and b, and another tubule).

Fig. 3) GTP-induced turn pairing observed on lipid nanorods. a) Molecular interactions between dynamin turns within the helix (yellow arrow) are resolved on a lipid nanorod. **b)** Distribution of the dynamin helix pitches on lipid nanorods before (grey bars, 15.4 ± 2.9nm; mean ± SD, *N*=4) and after (red bars, 10.8 ± 3.1nm, *N*=4) GTP-

addition. **c)** Dynamin helix images before (left) and after (right) GTP- showing a reduction of the helix pitch, with respective height profiles along the dotted lines (middle). Orange arrowhead point the lipid and white arrowhead dynamin polymerized. **d)** Dynamin helix images before (left) and after (right) GTP-addition showing an increase of the pitch, with respective height profiles along the dotted lines (middle).

Fig. 4) Dynamin helix turns relative displacements during constriction. a) Time-lapse sequence of zipper-like dissociation-association movements between neighboring ΔPRD-dynamin helix turns during GTP-hydrolysis. **b)** Time-lapse images and profile analysis of three ΔPRD-dynamin turns close to a fission site (F:P.2 in Fig. 2) on a DOPS tubule: positions of peaks in each turn are sequentially aligned and misaligned. Colors in lower panels correspond to height profiles of the same color. **c)** Transmission electron microscopy images of dynamin polymerized on stacked supported lipid bilayers before (left) and after (right) GTP-addition. **d)** Kymograph (left, along the red dashed line in image +58s) illustrating the relative movement of ΔPRD-dynamin oligomers on stacked planar membranes. Image sequence (right) displaying the morphological changes of the ΔPRD-dynamin coat on the supported lipid bilayer.

Fig. 1

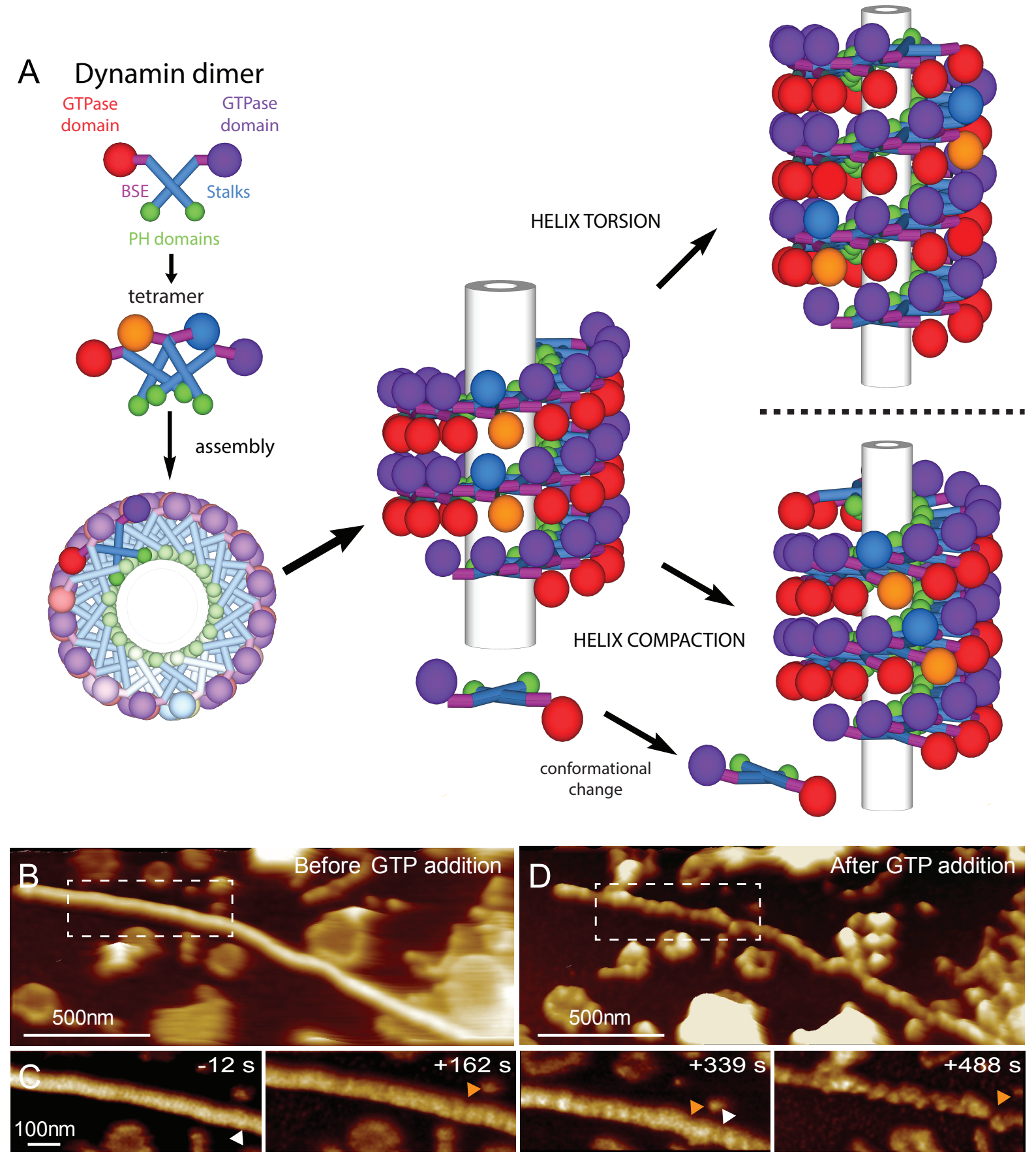
A
Dynamin dimer
GTPase domain
GTPase domain
BSE
Stalks
PH domains
tetramer
assembly
HELIX TORSION
HELIX COMPACTION
conformational change
B
Before GTP addition
500nm
D
After GTP addition
500nm
C
-12 s
+162 s
+339 s
+488 s
100nm

Fig. 2

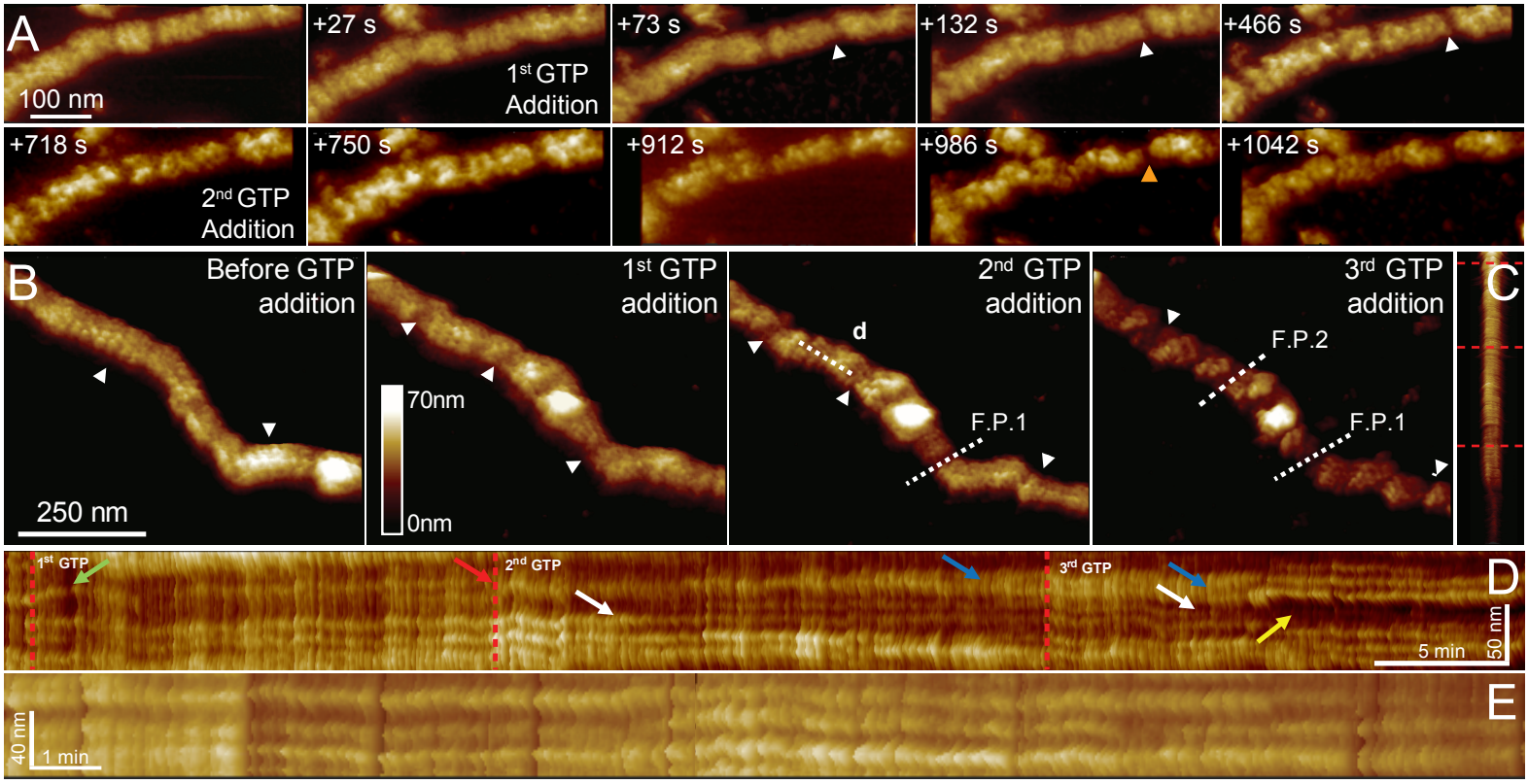
A
100 nm
+27 s
1st GTP Addition
+73 s
+132 s
+466 s
+718 s
2nd GTP Addition
+750 s
+912 s
+986 s
+1042 s
B
Before GTP addition
1st GTP addition
2nd GTP addition
3rd GTP addition
70nm
0nm
d
F.P.1
F.P.2
250 nm
C
D
1st GTP
2nd GTP
3rd GTP
5 min
50 nm
E
40 nm
1 min

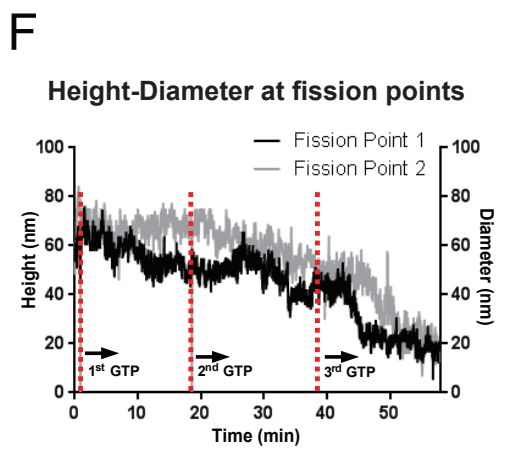
F
Height-Diameter at fission points
Fission Point 1
Fission Point 2
Height (nm)
Diameter (nm)
1st GTP
2nd GTP
3rd GTP
Time (min)

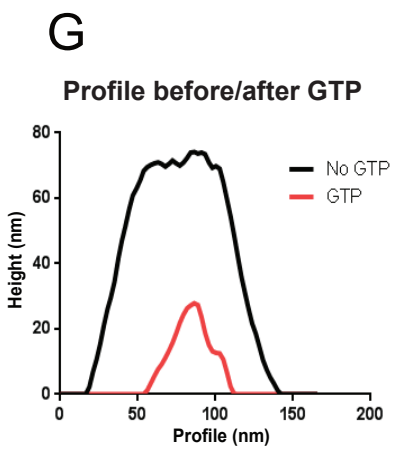
G
Profile before/after GTP
No GTP
GTP
Height (nm)
Profile (nm)

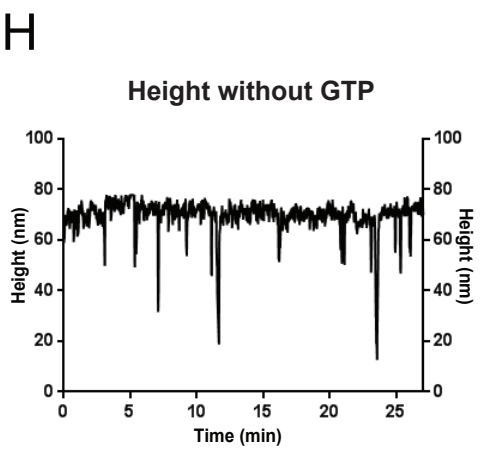
H
Height without GTP
Height (nm)
Time (min)

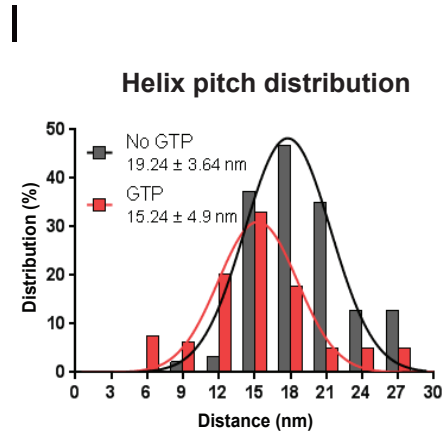
I
Helix pitch distribution
No GTP
19.24 ± 3.64 nm
GTP
15.24 ± 4.9 nm
Distribution (%)
Distance (nm)

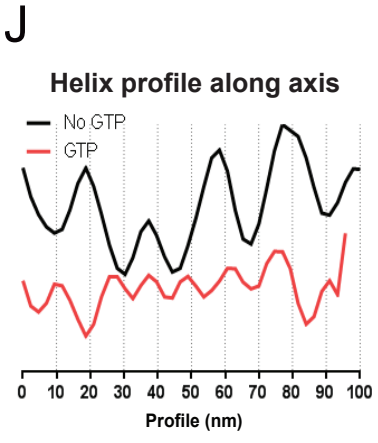
J
Helix profile along axis
No GTP
GTP
Profile (nm)

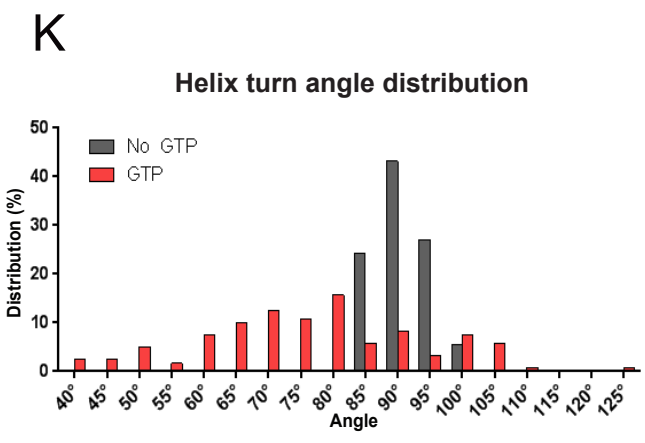
K
Helix turn angle distribution
No GTP
GTP
Distribution (%)
Angle

Fig. 3

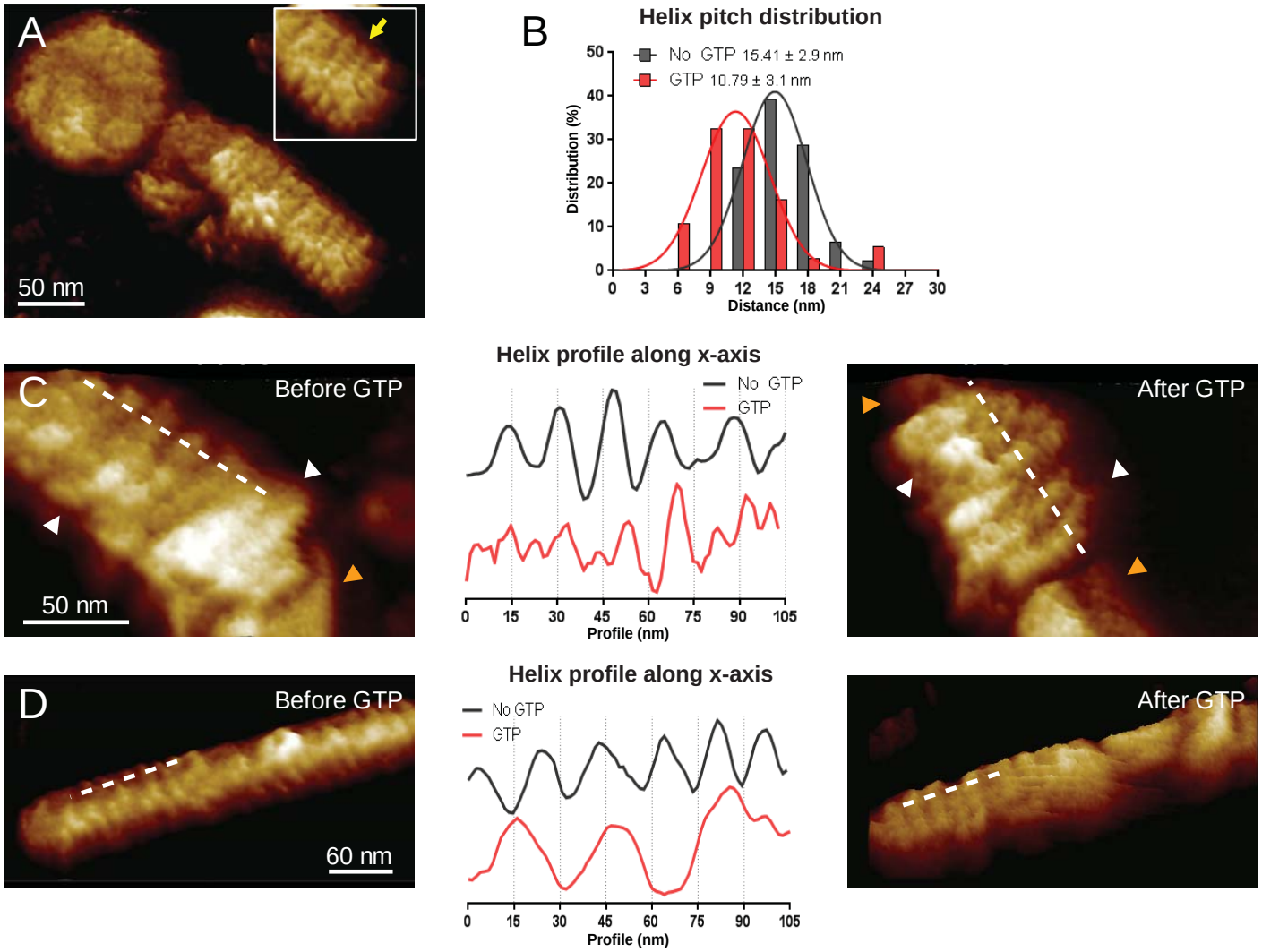
A
50 nm
B
Helix pitch distribution
No GTP 15.41 ± 2.9 nm
GTP 10.79 ± 3.1 nm
Distribution (%)
Distance (nm)
C
Before GTP
50 nm
Helix profile along x-axis
No GTP
GTP
Profile (nm)
After GTP
D
Before GTP
60 nm
Helix profile along x-axis
No GTP
GTP
Profile (nm)
After GTP

Fig. 4

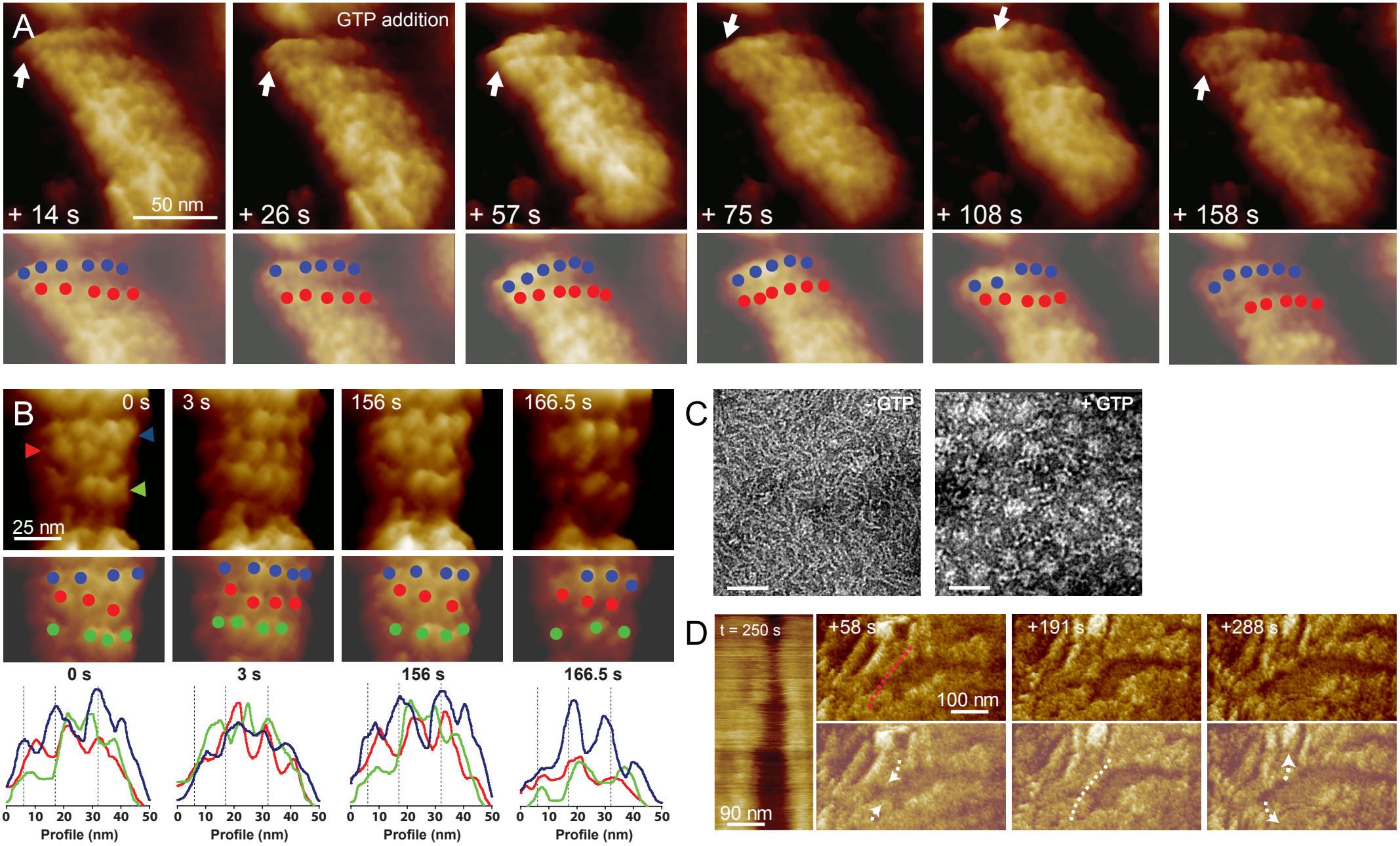
A
GTP addition
+ 14 s
50 nm
+ 26 s
+ 57 s
+ 75 s
+ 108 s
+ 158 s
B
0 s
3 s
156 s
166.5 s
25 nm
0 s
3 s
156 s
166.5 s
0 10 20 30 40 50
Profile (nm)
C
- GTP
+ GTP
D
t = 250 s
90 nm
+58 s
100 nm
+191 s
+288 s